Chinese Chemical Letters 34 (2023) 107690

Contents lists available at ScienceDirect

Chinese Chemical Letters

journal homepage: www.elsevier.com/locate/cclet

# Effect of poly(4–*tert*-butylstyrene) block length on the microphase structure of poly(ethylene oxide)-*b*-poly(4-vinylbenzyl chloride)-*b*-poly(4–*tert*-butylstyrene) triblock terpolymers

Kun An[a], Jia Gao[a], Yihang Chen[b], Jingjing Nie[c], Yongjin Li[b], Junting Xu[a], Binyang Du[a,*]

[a] State Key Laboratory of Motor Vehicle Biofuel Technology, Department of Polymer Science & Engineering, Zhejiang University, Hangzhou 310027, China
[b] College of Material, Chemistry and Chemical Engineering, Hangzhou Normal University, Hangzhou 310036, China
[c] Department of Chemistry, Zhejiang University, Hangzhou 310027, China

ARTICLE INFO

*Article history:*
Received 14 May 2022
Revised 8 July 2022
Accepted 17 July 2022
Available online 19 July 2022

*Keywords:*
ABC triblock terpolymer
Phase structure
SAXS
HPL
Thermodynamically stable

ABSTRACT

A series of linear poly(ethylene oxide)-*b*-poly(4-vinylbenzyl chloride)-*b*-poly(4–*tert*-butylstyrene) ($PEO_{113}$-*b*-$PVBC_{130}$-*b*-P*t*BS$_x$ or $E_{113}V_{130}T_x$) triblock terpolymers with various lengths $x$ (=20, 33, 66, 104, 215) of P*t*BS block were synthesized *via* a two-step reversible addition-fragmentation chain transfer (RAFT) polymerization. The $E_{113}V_{130}T_x$ triblock terpolymers were non-crystalline because the PVBC and P*t*BS blocks strongly hindered the crystallization of PEO block. The effects of P*t*BS block length $x$ on the phase structures of $E_{113}V_{130}T_x$ triblock terpolymers were investigated by combined techniques of small-angle X-ray scattering (SAXS) and transmission electron microscopy (TEM). It was found that with increasing $x$ from 20 to 215, the phase structure of $E_{113}V_{130}T_x$ triblock terpolymers became more ordered and changed from disordered structure, hexagonally-packed cylinder (HEX), hexagonally perforated layer (HPL), to lamellar (LAM) phase structures. Temperature-variable SAXS measurements showed that the HEX, HPL and LAM phase structures obtained for $E_{113}V_{130}T_{66}$, $E_{113}V_{130}T_{104}$ and $E_{113}V_{130}T_{215}$ by thermal annealing, respectively, were thermodynamically stable in the temperature range of 30–170 °C.

© 2023 Published by Elsevier B.V. on behalf of Chinese Chemical Society and Institute of Materia Medica, Chinese Academy of Medical Sciences.

Block copolymers (BCPs) are composed of two or more chemically and physically distinct linear chains with dozens to hundreds identical repeating units linked together covalently [1]. The precise control over the architecture, molecular weight, chemical composition of block copolymers and their characteristics of self-assembling into periodically ordered structures with domain size of 10–100 nm make BCPs fascinating nanostructured soft materials [2–5]. They have a great variety of potential applications in many emerging fields [6–9], such as nanophotonics [10,11], semiconductor microelectronics [12,13], energy and batteries [14,15]. The simplest and most studied architecture is the AB-type diblock copolymer. Phase behavior of block copolymer is determined by three primary factors: the degree of polymerization (N), Flory-Huggins parameter ($\chi$) and volume fraction (f) of each block [1]. Based on the self-consistent mean-field theory, Masten *et al.* predicted four stable equilibrium phases: spherical in a body-centered cubic lattice (BCC), hexagonally-packed cylinders (HEX), gyroid (GYR), and lamellae (LAM) [16]. Khandpur *et al.* proved the existence of the four equilibrium morphologies with studies of poly(isoprene-*b*-styrene) diblock copolymers, and observed the hexagonally perforated layer (HPL) phase, which was proved to be metastable actually, suggesting a good agreement between experimental results and phase diagram calculated by SCFT theory [17]. As a great amount of works have been published, additional phases, such as face-centered cubic (FCC) spheres [18], and A15 phase [19] have been sporadically observed in minute portions of the phase diagram. Studies of linear AB-type diblock copolymers experimentally and theoretically have laid a solid foundation for the investigation of phase behaviors of multiblock copolymers.

To explore more phase morphologies, a third C block is added to synthesize the linear ABC-type triblock terpolymers. With more primary factors than that of linear AB-type diblock copolymers, including $\chi_{BC}$, $\chi_{AC}$, $N_{BC}$, $N_{AC}$, $f$ and the block sequence, linear ABC-type phase behaviors become more complex and many phase morphologies have been predicted theoretically [20] or observed experimentally (over 30 phases have been identified to date in bulk). Taking the block sequence into consideration, linear ABC type can be defined as frustrated and non-frustrated systems. Without

* Corresponding author.
*E-mail address:* duby@zju.edu.cn (B. Du).

https://doi.org/10.1016/j.cclet.2022.07.033
1001-8417/© 2023 Published by Elsevier B.V. on behalf of Chinese Chemical Society and Institute of Materia Medica, Chinese Academy of Medical Sciences.

frustration ($\chi_{AC} \geq \chi_{BC} \geq \chi_{AB}$ ), ABC triblock terpolymers tend to form three-domain analogues of typical AB diblock morphologies. Matsushita *et al*. [21,22] synthesized a series of polyisoprene-*b*-polystyrene-*b*-poly(2-vinylpyridene) (ISP) triblock terpolymers ($\chi_{IP} \geq \chi_{SP} \geq \chi_{IS}$) and observed their phase morphologies by changing the volume fractions of the middle-block polymer. Tricontinuous alternating gyroid, three-domain four-layer lamella, cylindrical structure composed of two kinds of cylindrical domains, and spherical structure compose of two kinds of spherical domain were identified, which were similar to the four conventional equilibrium phases in AB-type diblock copolymers. Hiekkatalipale *et al*. [23] synthesized a series of polystyrene-*b*-polybutadiene-*b*-poly(*tert*–butyl methacrylate) (SBT) triblock terpolymers, and observed core-shell cylinder, lamella-lamella, cylinder-in-lamella, and core-shell gyroid morphologies. Core-shell structure and three-domain analogues occupied the majority of the phase diagram because the B block spread onto T block to prevent the unfavorable S/T interface ($\chi_{BT} << \chi_{ST}$). Frustrated ABC triblock terpolymers tend to form a great variety of novel phase morphologies and complex network structures. Krappe and his co-workers [24,25] conducted detailed studies on polystyrene-*b*-polybutadiene-*b*-poly(methyl methacrylate) (SBM) triblock terpolymers, and observed spheres on spheres, cylinders at cylinder, undulated/perforated cylinder in cylinder, and spheres on cylinder structure. Epps and his co-workers [26] carried out comprehensive studies on polyisoprene-*b*-polystyrene-*b*-poly(ethylene oxide) (ISO) triblock copolymers and observed orthorhombic $O^{70}$, alternating gyroid ($Q^{214}$), core-shell gyroid ($Q^{230}$) phase structures.

In the present work, a series of linear $PEO_{113}$-*b*-$PVBC_{130}$-*b*-P*t*$BS_x$ ($E_{113}V_{130}T_x$) triblock terpolymers were synthesized *via* a two-step reversible addition-fragmentation chain transfer (RAFT) polymerization by using poly(ethylene oxide) based chain transfer agent ($PEO_{113}$-CTA) as the first block, 4-vinylbenzyl chloride (VBC) and 4–*tert*-butylstyrene (*t*BS) as the monomers. PEO was chosen as first block because it was easily to synthesize PEO chain transfer agent for further RAFT polymerization. By choosing VBC and *t*BS as the second and third monomers can achieve $\chi_{VT} \gg \chi_{ET} > \chi_{EV}$. As a result, the obtained $E_{113}V_{130}T_x$ triblock terpolymers were the frustrated systems. It might be expected that $E_{113}V_{130}T_x$ triblock terpolymers can form rich phase structures depending on the P*t*BS block length *x*. Furthermore, PVBC block might be post-modified because benzyl chloride group is reactive. Five $E_{113}V_{130}T_x$ triblock terpolymers with various *x* (20, 33, 66, 104, 215) were synthesized for studying the effects of P*t*BS block length *x* on the phase behavior of the triblock terpolymers by combined techniques of small angle X-ray scattering (SAXS) and transmission electron microscopy (TEM). Hexagonally-packed cylinder (HEX), hexagonally perforated layer (HPL), lamellar (LAM) phase structures were observed for $E_{113}V_{130}T_{66}$, $E_{113}V_{130}T_{104}$ and $E_{113}V_{130}T_{215}$, respectively, after thermal annealing. To the best of our knowledge, the stable HPL phase structure was rarely observed for triblock terpolymers by simple thermal annealing.

Poly(ethylene oxide) ($PEO_{113}$-OH, $M_n = 5000$, $M_w/M_n = 1.05$) and 4-vinylbenzyl chloride (VBC, 98%) were purchased from Macklin. 4–*tert*-butylstyrene (*t*BS, 94%) was purchased from Alfa Aesar. VBC and *t*BS were purified through an alkaline alumina column (100–200 mesh) to remove inhibitor before use. 4-Cyano-4-(dodecylsulfanylthiocarbonyl)-sulfanyl pentanoic acid (CTA, 97%) was purchased from Aladdin and used as received. All other reagents, such as dichloromethane (DCM), tetrahydrofuran (THF) and toluene were of analytical grade and used as received.

CTA (2.02 g, 5 mmol) and oxalyl chloride (2.15 mL, 25 mmol) were added into a clean glass flask with 10 mL of dry DCM and stirred at room temperature under $N_2$ atmosphere until no gas bubble was generated. Excess reagents were then removed under vacuum, and the residue was redissolved in dry DCM (20 mL). The flask was immersed into an ice/water bath and 25 mL of $PEO_{113}$-OH solution (0.08 mol/L in DCM) was added into the flask dropwise for about 1 h. The ice/water bath was taken away after 2 h and the reaction continued for 24 h at room temperature. The reaction mixture was concentrated and precipitated with cold diethyl ether three times. The precipitates were dried at 40 °C under vacuum for 12 h to give PEO based chain transfer agent ($PEO_{113}$-CTA).

The preparation of poly(ethylene oxide-*b*-4-vinylbenzyl chloride) ($PEO_{113}$-*b*-$PVBC_{130}$) diblock copolymer was carried out by traditional RAFT method. Typically, $PEO_{113}$-CTA (0.50 g, 0.1 mmol), VBC (15.26 g, 0.1 mol), and azobisisobutyronitrile (AIBN, 1.64 mg, 0.01 mmol) were added in a 50-mL Schlenk flask containing 5.0 mL 1,4-dioxane and stirred under nitrogen atmosphere. After the mixture was dissolved completely, three freezing-pumping-thawing cycles were performed. The Schlenk flask was then transferred to an oil bath at 80 °C for polymerization. After 1 h, the reaction was terminated by freezing with liquid nitrogen. The reaction mixture was precipitated with methanol for three times and the obtained diblock copolymers were dried at 40 °C under vacuum for 12 h.

A similar RAFT procedure was used to synthesize the triblock terpolymers, $PEO_{113}$-*b*-$PVBC_{130}$-*b*-P*t*$BS_x$. Typically, the diblock copolymer $PEO_{113}$-*b*-$PVBC_{130}$ obtained above (0.50 g, 0.019 mmol), *t*BS (4.58 g, 28.55 mmol) and AIBN (0.31 mg, 0.0019 mmol) were added in a 50-mL Schlenk flask containing 5.0 mL toluene and stirred under nitrogen atmosphere. After the mixture was dissolved completely, three freezing-pumping-thawing cycles were performed. The Schlenk flask was then transferred to an oil bath at 90 °C for polymerization, and the reaction was terminated by freezing with liquid nitrogen after 1 h. The reaction mixture was dialyzed against THF for 3 days at room temperature using a dialysis membrane (MWCO 8000). The obtained solution was concentrated by rotary evaporation. The solid product was then dried at 40 °C under vacuum for 12 h. The triblock terpolymers $PEO_{113}$-*b*-$PVBC_{130}$-*b*-P*t*$BS_x$ were abbreviated to be $E_{113}V_{130}T_x$, where the capital letters E, V, T represent the PEO, PVBC, and P*t*BS blocks, respectively, and the subscript *x* represents the polymerization degree of P*t*BS block.

Gel permeation chromatography (GPC) was performed to determine the molecular weight distribution ($M_w/M_n$) of $E_{113}V_{130}T_x$ triblock terpolymers by using a Waters GPC system calibrated with standard polystyrenes. It was measured with an elution rate of 1.0 mL/min using THF as the eluent. $^1$H NMR spectra of $E_{113}V_{130}T_x$ triblock terpolymers were recorded on a Bruker DMX-400 MHz instrument running at room temperature with tetramethylsilane (TMS) as the internal standard and $CDCl_3$ as the solvent. Differential scanning calorimetry (DSC) measurements were conducted using a TA Q200 instrument. Typically, 3–4 mg of $E_{113}V_{130}T_x$ samples were sealed in an aluminum pan, which was first heated to 180 °C for about 5 min to erase the thermal history of samples and then cooled to −80 °C and reheated to 180 °C. The heating and cooling rates were 10 °C/min. The data curve of second heating procedure was taken for analysis. Thermogravimetric analysis (TGA) was conducted on a TA Q50 thermogravimeter under a nitrogen atmosphere with a heating rate of 10 °C/min and a nitrogen flow rate of 20 mL/min.

Temperature-variable small-angle X-ray scattering (SAXS) measurements of $E_{113}V_{130}T_x$ triblock terpolymers were performed at BL16B1 beamline in Shanghai Synchrotron Radiation Facility (SSRF), China. The wavelength of the X-ray is 1.24 Å and the sample-to-detector distance was set as 2000 mm. The $E_{113}V_{130}T_x$ triblock terpolymers were dissolved in chloroform to obtain clear solutions with a concentration of 1% w/v. The polymer solutions were slowly dried by evaporating $CHCl_3$ at room temperature for one week. The obtained films were annealed under vacuum at 180 °C for 24 h. The annealed samples were then used for SAXS measurements. Samples were heated to the setting temperature by using a Linkam hot

**Table 1**
Characterization Data of $E_{113}V_{130}T_x$.

| Bulk sample | $M_n$[a] (kg/mol) | $M_w/M_n$[b] | $f_E$[c] | $f_V$[c] | $f_T$[c] | Phase structure[d] |
|---|---|---|---|---|---|---|
| $E_{113}V_{130}T_{20}$ | 28.2 | 1.23 | 17.0 | 70.0 | 13.0 | DIS |
| $E_{113}V_{130}T_{33}$ | 30.4 | 1.20 | 15.7 | 64.5 | 19.8 | DIS |
| $E_{113}V_{130}T_{66}$ | 35.7 | 1.25 | 13.1 | 53.9 | 33.0 | HEX |
| $E_{113}V_{130}T_{104}$ | 41.8 | 1.27 | 11.0 | 45.3 | 43.7 | HPL |
| $E_{113}V_{130}T_{215}$ | 59.4 | 1.30 | 7.5 | 30.9 | 61.6 | LAM |

[a] Determined by $^1$H NMR.
[b] Determined from GPC.
[c] $f_O$, $f_S$, $f_T$ were the volume fractions of PEO, PS and P*t*BS blocks of the triblock terpolymer, respectively. The densities of amorphous PEO, PVBC and P*t*BS [27] are 1.15, 1.09 and 0.95 g/cm$^3$, respectively.
[d] Determined by SAXS.

stage with a heating rate of 10 °C/min and then held for 2 min under nitrogen atmosphere before SAXS measurements. The exposure time was set as 20 s for data acquisition. The scattering vector was calibrated with the bull tendon. The two-dimensional (2D) SAXS patterns and one-dimension (1D) SAXS profiles were obtained by Fit2d software.

Transmission electron microscopy (TEM) measurements were performed by using a Hitachi HT-7700 TEM operated at 80 kV. TEM sample slices with thickness of *ca.* 50 nm were obtained by embedding the annealed $E_{113}V_{130}T_x$ triblock terpolymers in epoxy resin and then ultramicrotoming at about −120 °C using a Leica EM UC7 microtome. The sample slices were collected on copper grids and stained with osmium tetroxide ($OsO_4$) and ruthenium tetroxide ($RuO_4$) aqueous solutions (0.5% stabilized aqueous solution) for 4 h, respectively, before TEM observation.

In order to study effects of P*t*BS (T) block length on the phase structure of $E_{113}V_{130}T_x$ triblock terpolymers, five $E_{113}V_{130}T_x$ triblock terpolymers with the same polymerization degrees of E and V blocks and different polymerization degrees of the third T block were synthesized *via* a two-step RAFT process, as summarized in Scheme S1 (Supporting information). The number-average molecular weights ($M_n$) and volume fractions of each block ($f_E$, $f_V$ and $f_T$) of $E_{113}V_{130}T_x$ triblock terpolymers were determined by $^1$H NMR spectra, as shown in Fig. S1 (Supporting information). The molecular weight distributions ($M_w/M_n$) of $E_{113}V_{130}T_x$ triblock terpolymers were measured by GPC, as shown in Fig. S2 (Supporting information). The GPC traces indicated that the five triblock terpolymers exhibited relatively narrow molecular weight distribution. Table 1 summarized the values of $M_n$, $M_w/M_n$, $f_E$, $f_V$ and $f_T$ of five $E_{113}V_{130}T_x$ triblock terpolymers studied here [27].

TGA measurements were carried out to determine the degradation temperature and thermal stability of the triblock terpolymers. Fig. S3 (Supporting information) shows the TGA curves of $E_{113}V_{130}T_x$ triblock terpolymers. The temperature with 5% of weight loss was set as degradation temperature. The degradation temperature of $E_{113}V_{130}T_{104}$ triblock terpolymer was determined to be about 240 °C. All $E_{113}V_{130}T_x$ triblock terpolymers exhibited similar degradation temperature. Therefore, the following DSC and SAXS experiments were conducted below 240 °C to avoid the degradation of triblock terpolymers

DSC experiments were conducted to measure the glass transition temperature of $E_{113}V_{130}T_x$ triblock terpolymers and investigate the crystallization behavior of PEO block. Fig. S4 (Supporting information) shows the DSC curves of five $E_{113}V_{130}T_x$ triblock terpolymers. No melting endothermic peak was observed for the five triblock terpolymers, suggesting that the PEO block of $E_{113}V_{130}T_x$ was non-crystalline. These results indicated that PVBC and P*t*BS blocks hindered the crystallization of PEO block in $E_{113}V_{130}T_x$ triblock terpolymers. For $E_{113}V_{130}T_x$ triblock terpolymers with $x = 20$, 33, 66 and 104, only one glass transition temperature was observed and the $T_g$ values were smaller than those of the PVBC and P*t*BS homopolymers. The Flory-Huggins parameters of PEO and PVBC blocks ($\chi_{EV}$), PEO and P*t*BS blocks ($\chi_{ET}$), PVBC and P*t*BS blocks ($\chi_{VT}$) can be estimated by Hildebrand and Scoff equation [28]:

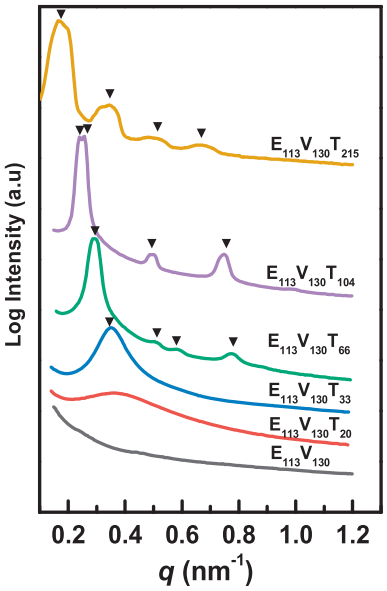


**Fig. 1.** SAXS profiles of $E_{113}V_{130}T_{20}$, $E_{113}V_{130}T_{33}$, $E_{113}V_{130}T_{66}$, $E_{113}V_{130}T_{104}$ and $E_{113}V_{130}T_{215}$ triblock terpolymers at 30 °C.

$$\chi_{AB} = \frac{\nu_{ref}}{RT}(\delta_A - \delta_B)^2 \quad (1)$$

where $\nu_{ref}$ is the segment volume, which can be calculated by $\nu_{ref} = (\nu_A \nu_B)^{1/2}$. $\nu_A$ and $\nu_B$ are specific volumes of block A and B, and it can be calculated by $\nu = M/\rho$, where $M$ is the molecular weight of each block and $\rho$ is the density of monomer. $R$ is the gas constant, 8.314 J mol$^{-1}$ K$^{-1}$. T is the absolute temperature. $\delta_A$ and $\delta_B$ are the Hilderbrand solubility parameters of block A and B. The specific volumes of PEO ($\nu_E$), PVBC ($\nu_V$) and P*t*BS ($\nu_T$) blocks were about 39.11, 140 and 169 cm$^3$/mol, respectively. The solubility parameters of PEO ($\delta_E$), PVBC ($\delta_V$) [29] and P*t*BS ($\delta_T$) [30] were 19.1, 20.24 and 16.6 (J/cm$^3$)$^{1/2}$, respectively. The Flory-Huggins parameters $\chi_{EV}$, $\chi_{ET}$, and $\chi_{VT}$ were then calculated to be about 0.045, 0.064 and 0.822 at 298 K. The values of $\chi_{EV}$ and $\chi_{ET}$ indicated that the PEO block showed good compatibility with PVBC and P*t*BS blocks, respectively, leading to the observation of single $T_g$ for $E_{113}V_{130}T_x$ triblock terpolymers with $x = 20$, 33, 66 and 104. However, when the P*t*BS block was long enough ($x = 215$), the second $T_g$ was observed and its value is 123 °C, which is similar to the reported $T_g$ of P*t*BS homopolymer ($T_g = 130$ °C [31]).

The phase structures of $E_{113}V_{130}T_x$ triblock terpolymers were investigated by SAXS and TEM. Fig. 1 shows the SAXS profiles of $E_{113}V_{130}T_x$ triblock terpolymers with various lengths of P*t*BS block ($x = 20$, 33, 66, 104, 215) at 30 °C and the corresponding $E_{113}V_{130}$ diblock copolymer. No scattering peak was observed for $E_{113}V_{130}$, suggesting that the phase structure of $E_{113}V_{130}$ was totally disordered. For $E_{113}V_{130}T_{20}$ and $E_{113}V_{130}T_{33}$, a broad scattering peak was observed from their SAXS profiles, suggesting that $E_{113}V_{130}T_{20}$ and $E_{113}V_{130}T_{33}$ exhibited disordered phase structure (DIS). The scattering peak of $E_{113}V_{130}T_{33}$ was stronger and sharper than that of $E_{113}V_{130}T_{20}$. For $E_{113}V_{130}T_{66}$, four scattering peaks were observed at $q/q^* = 1$, $3^{1/2}$, 2, $7^{1/2}$ with the primary scattering peak centered at $q^* = 0.287$ nm$^{-1}$, indicating that $E_{113}V_{130}T_{66}$ exhibited a hexagonally packed cylindrical (HEX) phase structure. For $E_{113}V_{130}T_{215}$, four scattering peaks were observed at $q/q^* = 1$, 2, 3, 4 with the primary scattering centered at $q^* = 0.164$ nm$^{-1}$, indicating that $E_{113}V_{130}T_{215}$ exhibited a lamellar (LAM) phase struc-

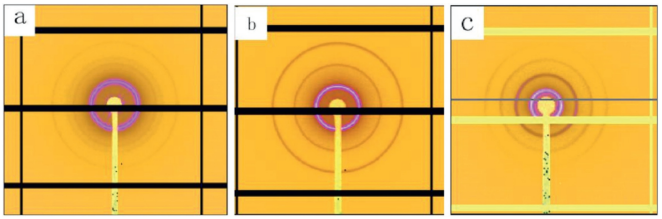


**Fig. 2.** 2D SAXS patterns of (a) $E_{113}V_{130}T_{66}$, (b) $E_{113}V_{130}T_{104}$ and (c) $E_{113}V_{130}T_{215}$ at 30 °C.

ture. Interestingly, for $E_{113}V_{130}T_{104}$, four scattering peaks were observed at $q = 0.239$, 0.253, 0.489 and 0.729 $nm^{-1}$. These scattering peaks can be indexed according to a hexagonally perforated lamellar (HPL) structure by calculating the crystal surface spacing $d_{hkl}$ of the hexagonal lattice [32]:

$$\frac{1}{d_{hkl}} = \frac{4}{3}\left(\frac{h^2 + hk + k^2}{a^2}\right) + \frac{l^2}{c^2} \quad (2)$$

where $h$, $k$, $l$ are the Miller indices, and $a$, $c$ are lattice parameters of the unit cell. The four observed scattering peaks can be indexed as (101), (003), (105), (215) by adopting a trigonal ABCABC… stacking sequence with $a = 32.5$ nm, $c = 73.4$ nm. The obtained lattice parameter ratio $c/a$ was 2.25, which is similar to those reported in literature for HPL phase structure [33,34] with the same trigonal ABCABC… stacking sequence. Loo *et al.* [35] observed a highly regular HPL structure in polystyrene-poly(ethylene-*alt*-propylene) diblock copolymer with the ratio $c/a = 2.24$. Zin *et al.* [33] observed a shear-induced HPL structure in polystyrene-polyisoprene diblock copolymer with the ratio $c/a = 2.20$. The above results indicated that the phase structure of $E_{113}V_{130}T_x$ triblock terpolymers became more ordered with increasing the length $x$ of P*t*BS block. With increasing $x$ from 20 to 215, the phase structure of $E_{113}V_{130}T_x$ triblock terpolymers changed from disordered structure, HEX, HPL to LAM phase structures. The Flory-Huggins parameter $\chi_{VT}$ (0.822) was much larger than $\chi_{EV}$ (0.045) and $\chi_{ET}$ (0.064). The relationship of $\chi_{VT} \gg \chi_{ET} > \chi_{EV}$ indicated that the $E_{113}V_{130}T_x$ triblock terpolymers were frustrated systems [34], meaning that more E/T interfaces could occur easily. Increasing the length of P*t*BS block will thus enhance the phase separation of $E_{113}V_{130}T_x$ triblock terpolymers, leading to the formation of enhanced ordered phase structures.

The corresponding 2D SAXS patterns of $E_{113}V_{130}T_{66}$, $E_{113}V_{130}T_{104}$, and $E_{113}V_{130}T_{215}$ were showed in Fig. 2. The 2D SAXS patterns containing whole circles suggested that the formed HEX, HPL, and LAM structures were highly ordered and isotropic. The HEX and LAM phase structures are thermodynamic equilibrium phases for block copolymers and can be obtained by thermal annealing [36]. However, the HPL phase was usually obtained by shearing the melt sample of block copolymer because the HPL phase is considered to be thermodynamically metastable [37–39]. In the present work, the 2D SAXS pattern and 1D SAXS profile indicated that the HPL structure was obtained for $E_{113}V_{130}T_{104}$ only by thermal annealing without any shearing, which might suggest that the HPL phase of $E_{113}V_{130}T_{104}$ was thermodynamically stable.

To further investigate the stability of HEX, HPL and LAM phases formed for $E_{113}V_{130}T_{66}$, $E_{113}V_{130}T_{104}$, and $E_{113}V_{130}T_{215}$, respectively, the evolution of phase structure with increasing temperature were studied by SAXS. Fig. S5 (Supporting information) shows the SAXS profiles of $E_{113}V_{130}T_{66}$, $E_{113}V_{130}T_{104}$, and $E_{113}V_{130}T_{215}$ at various temperatures. It can be seen from Fig. S5 that the SAXS profiles of $E_{113}V_{130}T_{66}$, $E_{113}V_{130}T_{104}$, and $E_{113}V_{130}T_{215}$ were almost unchanged in the temperature range of 30 °C to 170 °C. No order-to-disorder transition and order-to-order transition were observed. These results indicated that the HEX, HPL and LAM phase structures of $E_{113}V_{130}T_x$ triblock terpolymers obtained by thermal-annealing were thermodynamically stable at 30–170 °C.

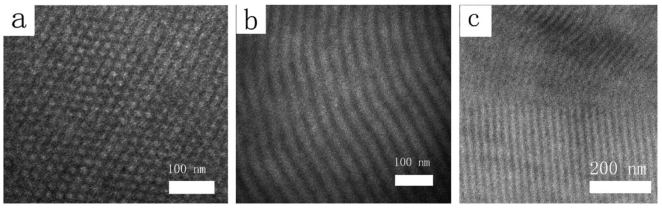


**Fig. 3.** TEM images of (a) $E_{113}V_{130}T_{66}$, (b) $E_{113}V_{130}T_{215}$ and (c) $E_{113}V_{130}T_{104}$.

The phase morphologies of $E_{113}V_{130}T_{66}$, $E_{113}V_{130}T_{104}$, and $E_{113}V_{130}T_{215}$ triblock terpolymers were further verified by TEM observation, as shown in Fig. 3. The PEO and PVBC blocks were stained dark with $RuO_4$ and $OsO_4$, respectively. For $E_{113}V_{130}T_{66}$, the HEX morphology with the smaller P*t*BS block packing into the interiors of cylinders was observed (Fig. 3a). The domain spacing measured from TEM image was about 20.8 nm, which was close to the value of 21.9 nm calculated by $d = 2\pi/q^*$ from the corresponding SAXS profile. For $E_{113}V_{130}T_{215}$, the lamellar morphology containing light and dark stripes was observed (Fig. 3b). The domain spacing of LAM morphology from TEM image was about 36.8 nm, which was in good agreement with that of 38.3 nm obtained from SAXS profiles. For $E_{113}V_{130}T_{104}$, the alternate lamellae perpendicular to the projection of perforated layers without perforations were observed (Fig. 3c). The domain spacing of perforated layers from TEM image was about 26.3 nm, which well agreed with that of 26.3 nm determined from SAXS profiles. However, we were not able to observe the regions where the lamellae were perforated by hexagonally arranged domains. Nevertheless, the TEM images were consistent with the SAXS results.

In summary, a series of $E_{113}V_{130}T_x$ triblock terpolymers with the same lengths of PEO (E) and PVBC (V) blocks but various lengths $x$ (20, 33, 66, 104, 215) of P*t*BS (T) block were synthesized *via* a two-step RAFT process. The obtained $E_{113}V_{130}T_x$ triblock terpolymers were non-crystalline because the PVBC and P*t*BS blocks strongly hindered the crystallization of PEO block. With increasing $x$ from 20 to 215, the phase structure of $E_{113}V_{130}T_x$ triblock terpolymers became more ordered and changed from disordered structure, HEX, HPL to LAM phase structures. Such HEX, HPL and LAM phase structures of $E_{113}V_{130}T_x$ triblock terpolymers obtained by thermal-annealing were thermodynamically stable in the temperature range of 30–170 °C.

## Declaration of competing interest

The authors declare that they have no known competing financial interests or personal relationships that could have appeared to influence the work reported in this paper.

## Acknowledgment

The authors thank the National Natural Science Foundation of China (Nos. 21875214, 21674097 and 21774111) for financial support and the beamline BL16B1 at SSRF for providing the beam time.

## Supplementary materials

Supplementary material associated with this article can be found, in the online version, at doi:10.1016/j.cclet.2022.07.033.

## References

[1] F.S. Bates, M.A. Hillmyer, T.P. Lodge, et al., Science 336 (2012) 434–440.

[2] F.S. Bates, G.H. Fredrickson, Phys. Today 52 (2000) 32–38.
[3] V. Castelletto, I.W. Hamley, Curr. Opin. Solid State Mater. Sci. 8 (2004) 426–438.
[4] Y.L. Cao, Y. Shi, X.H. Wu, et al., Chin. Chem. Lett. 31 (2020) 1660–1664.
[5] Y.W. Deng, H. Chen, X.F. Tao, et al., Chin. Chem. Lett. 31 (2020) 1931–1935.
[6] L. Yang, P. Liu, C.C. Zhu, et al., Chin. Chem. Lett. 32 (2021) 822–825.
[7] L. Zeng, Z.P. Su, X.Y. Li, et al., Chin. Chem. Lett. 31 (2020) 3131–3134.
[8] Z.W. Jiang, Y.S. Wang, G.Q. Xu, et al., Chin. Chem. Lett. 33 (2022) 1011–1016.
[9] J. Ren, X. Shu, Y. Wang, et al., Chin. Chem. Lett. 33 (2022) 1650–1658.
[10] M. Stefik, S. Guldin, S. Vignolini, et al., Chem. Soc. Rev. 44 (2015) 5076–5091.
[11] J. Yoon, W. Lee, E.L. Thomas, MRS Bull. 30 (2005) 721–726.
[12] C.M. Bates, M.J. Maher, D.W. Janes, et al., Macromolecules 47 (2014) 2–12.
[13] C. Sinturel, F.S. Bates, M.A. Hillmyer, ACS Macro Lett. 4 (2015) 1044–1050.
[14] H. Hoppe, N.S. Sariciftci, J. Mater. Res. 19 (2004) 1924–1945.
[15] N. Sary, F. Richard, C. Brochon, et al., Adv. Mater. 22 (2010) 763–768.
[16] F.S. Bates, Science 251 (1991) 898–905.
[17] A.K. Khandpur, S. Foerster, F.S. Bates, et al., Macromolecules 28 (1995) 8796–8806.
[18] Y.Y. Huang, J.Y. Hsu, H.L. Chen, et al., Macromolecules 40 (2007) 406–409.
[19] M.W. Bates, J. Lequieu, S.M. Barbon, et al., Proc. Natl. Acad. Sci. 116 (2019) 13194–13199.
[20] A.B. Chang, F.S. Bates, Macromolecules 53 (2020) 2765–2768.
[21] Y. Mogi, M. Nomura, H. Kotsuji, et al., Macromolecules 27 (1994) 6755–6760.
[22] Y. Mogi, K. Mori, H. Kotsuji, et al., Macromolecules 26 (1993) 5169–5173.
[23] T.I. Löbling, P. Hiekkataipale, A. Hanisch, et al., Polymer (Guildf) 72 (2015) 479–489.
[24] U. Breiner, U. Krappe, V. Abetz, et al., Macromol. Chem. Phys. 198 (1997) 1051–1083.
[25] U. Breiner, U. Krappe, T. Jakob, et al., Polym. Bull. 40 (1998) 219–226.
[26] T.S. Bailey, C.M. Hardy, T.H. Epps, et al., Macromolecules 35 (2002) 7007–7017.
[27] J.E. Mark, Physical Properties of Polymers Handbook, 2nd Ed., Springer, New York, 2007.
[28] T.M. Madkour, Chem. Phys. 274 (2001) 187–198.
[29] A.F.M. Barton, Handbook of Polymer-Liquid Interaction Parameters and Solubility Parameters, 1st Ed., Routledge, New York, 2018.
[30] P.J. Griffin, G.B. Salmon, J. Ford, et al., J. Polym. Sci. Part B: Polym. Phys. 54 (2016) 254–262.
[31] B. Wu, M. Zhou, D. Lu, Iran. Polym. J. 15 (2006) 989–995.
[32] C. Hammond, The Basics of Crystallography and Diffraction, 4th Ed., Oxford University Press, Oxford, 2015.
[33] J.H. Ahn, W.C. Zin, Macromolecules 32 (2000) 641–644.
[34] S. Förster, A.K. Khandpur, J. Zhao, et al., Macromolecules 27 (1994) 6922–6935.
[35] Y.L. Loo, R.A. Register, D.H. Adamson, et al., Macromolecules 38 (2005) 4947–4949.
[36] L. Zhu, P. Huang, W.Y. Chen, et al., Macromolecules 36 (2003) 3180–3188.
[37] N. Zhou, T.P. Lodge, F.S. Bates, Soft Matter 6 (2010) 1281–1290.
[38] S.E. Mastroianni, J.P. Patterson, R.K. O'Reilly, et al., Soft Matter 9 (2013) 10146–10154.
[39] J. Gao, C. Lv, K. An, et al., Macromolecules 53 (2020) 9641–9653.